JOURNAL OF COMPUTATIONAL PHYSICS 102, 139–159 (1992)

A Comparative Study of Advanced Shock-Capturing Schemes Applied to Burgers' Equation

H. Q. YANG AND A. J. PRZEKWAS

CFD Research Corporation, 3325-D Triana Boulevard, Huntsville, Alabama 35805

Received February 23, 1990; revised January 14, 1991

In recent years, a number of new shock-capturing finite difference schemes, often called high resolution schemes, have been proposed. We have considered several variations of the TVD and FCT schemes and geometrical approaches such as MUSCL, ENO, and PPM. Included is an organized overview and classification of the schemes. Only essential features are described, and numerical implementation is discussed. Much of the mathematical theory is omitted, but a key source reference list is provided. In this paper we present a comparative study of these schemes applied to the Burgers' equation. The objective is to assess their performance for problems involving formation and propagation of shocks, shock collisions, and expansion of discontinuities.

1. INTRODUCTION

The challenge of the numerical solution of hyperbolic conservation equations is to obtain high accuracy of the solution in both discontinuous (shock waves and contact discontinuities) and smooth regions. The upwind finite-difference scheme, as generally known, can eliminate possible spurious oscillations in the neighborhood of shock waves and can guarantee the resolution of discontinuities without wiggles. But it possesses a strong numerical dissipation which spreads discontinuities over many grid points, and it produces a low accuracy in the smooth region of the solution. The central difference scheme, on the other hand, gives good resolution in smooth regions, but introduces the spurious oscillations near steep gradients, and sometimes leads to nonlinear instability.

To remedy the above difficulties, various new shock-capturing schemes have been developed in recent years. These schemes, usually called "high resolution schemes," have the following properties: they are at least of second-order accuracy in the smooth part of the solution; they sharply resolve discontinuities without generating spurious oscillations; and in contrast to classical second or higher order scheme, they do not need a priori specified artificial viscosity. The basic concept behind all these high resolution schemes is to use a higher order scheme as much as possible and in the meantime to intelligently add sufficient dissipation in the localized steep gradient region to eliminate possible numerical oscillation. It is this adaptive dissipation property that distinguishes the modern (new) and classical (old) shock-capturing schemes. As a result, the modern shock-capturing schemes are nonlinear even when they are applied to linear problems.

The purposes of this paper are:

(1) to summarize the similarities, differences, and properties of the modern shock-capturing schemes; and

(2) to compare their performances in solving the nonlinear equations.

The modern shock-capturing schemes considered in this paper are: second-order TVD scheme of Roe [1, 2] and Sweby [3]; upwind TVD of Harten [4] and Yee *et al.* [5]; symmetric TVD of Yee [6, 7] and Davis [8]; one-parameter family TVD of Chakravarthy and Osher [9]; ENO scheme of Harten *et al.* [10, 11]; FCT schemes of Zalesak [12] and McDonald and Ambrosiano [13]; MUSCL schemes of van Leer [14], Goodman and LeVeque [15], Davis [16], and Colella [17]; and PPM of Colella and Woodward [18].

Recently, Zalesak [19] has classified advanced schemes and assessed their performance on a one-dimensional linear advection in which many of the TVD and MUSCL schemes are equivalent. Also a comprehensive review of the TVD schemes for scalar and for systems of equations has been consolidated by Yee [7, 20], and an excellent assessment of the schemes for the shock tube problems has been reported. Van Leer [21] presented another comparative study on the upwind-differencing schemes of Godunov, Engquist and Osher, and Roe.

In this paper one-dimensional inviscid Burgers' equation is taken as the test problem due to its properties pertinent to nonlinear wave propagation. Two test cases are considered: one is the propagation of an initial sine wave and the another one is the propagation of an initial discontinuous curve which involves shock collision and expansion of dis-

0021-9991/92 $5.00

continuities. Since the equation is nonlinear, a consequence of the changing wave speed results in the coalescence of characteristics and the formation of discontinuous solutions which are similar to the shock waves in fluid dynamics. The assessment of the numerical schemes is based on the examination of the accuracy of predicting such nonlinear effects as: formation of shocks; propagation of shocks; expansion of discontinuities; and collision of shocks. As shown in the paper, some of the promoted and well-performing schemes for the linear equation may be inadequate for the nonlinear problems.

The paper first describes the essential details of various schemes and their numerical formulation and then presents the comparisons and physical insights of two test cases of Burgers' equation. The conclusions are drawn in the last part of the paper.

2. DESCRIPTIONS OF MODERN SHOCK-CAPTURING SCHEMES

In this paper, we consider the numerical solution of initial value problems for hyperbolic conservation laws:

$$u_t + f_x = 0. \tag{2.1}$$

Here $u(x, t)$ is an unknown function and $f(u)$ is called flux function. Before introducing the finite-difference formulation, we need to define our discretization nomenclature and indexing practices. We will restrict the discussion to one-dimensional problems. Figure 1 illustrates our x–t grid and the indexing practice.

Integrating the conservation equation (2.1) within the i-control volume $(x_{i+1/2} - x_{i-1/2})$ for $t^n < t < t^{n+1}$, we obtain

$$\int_{x_{i-1/2}}^{x_{i+1/2}} u(x, t^{n+1})\, dx = \int_{x_{i-1/2}}^{x_{i+1/2}} u(x, t^n)\, dx - \int_{t^n}^{t^{n+1}} f[u(x_{i+1/2}, t)]\, dt + \int_{t^n}^{t^{n+1}} f[u(x_{i-1/2}, t)]\, dt. \tag{2.2}$$

The discrete nature of the problem forces us to replace the exact integrals by the average values for the dependent variables u_i^n and u_i^{n+1},

$$u_i^{n+1} = u_i^n - \frac{\Delta t}{\Delta x}(F_{i+1/2} - F_{i-1/2}), \tag{2.3}$$

where $\Delta x = x_{i+1/2} - x_{i-1/2}$ and will be taken as constant unless otherwise stated and $\Delta t = t^{n+1} - t^n$. $F_{i+1/2}$ and $F_{i-1/2}$ are called transportive fluxes and are functions of f, at one

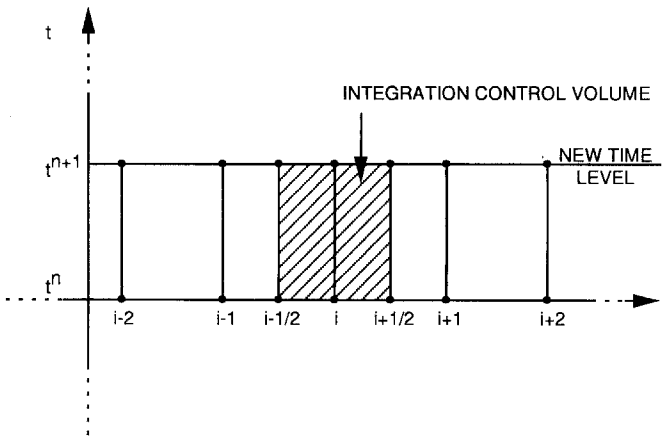

FIG. 1. Computational grid, indexing practice.

or more of the time levels. With known u at time level t^n, the key to finding the solution at new time level, u_i^{n+1}, is to properly compute the interface fluxes, $F_{i+1/2}$ and $F_{i-1/2}$. In the following, we will discuss the major issues in calculating the $F_{i+1/2}$ for different shock-capturing schemes.

2.1. Classical Diffusive and Dispersive Schemes

The three classical schemes (namely: upwind, central, and Lax–Wendroff) use different assumptions for calculating the interface fluxes (Eq. (2.3)). The first-order upwind scheme uses:

$$F_{i+1/2}^{\mathrm{UP}} = \tfrac{1}{2}(f_{i+1} + f_i) - \tfrac{1}{2}\,\mathrm{sign}(a_{i+1/2})(f_{i+1} - f_i) \tag{2.4}$$

or

$$F_{i+1/2}^{\mathrm{UP}} = \tfrac{1}{2}(f_{i+1} + f_i) - \tfrac{1}{2}|a_{i+1/2}|\,\Delta_{i+1/2}, \tag{2.5}$$

where

$$\Delta_{i+1/2} = u_{i+1} - u_i. \tag{2.6}$$

The wave speed, a, is computed as

$$a_{i+1/2} = \begin{cases} \dfrac{(f_{i+1} - f_i)}{\Delta_{i+1/2}} & \text{if } \Delta_{i+1/2} \neq 0 \\ \dfrac{\partial f}{\partial u} & \text{otherwise.} \end{cases} \tag{2.7}$$

Equation (2.5) may not satisfy the entropy condition, so that $|a_{i+1/2}|$ is replaced by $\psi(a_{i+1/2})$ which is defined as

$$\psi(a_{i+1/2}) = \max(|a_{i+1/2}|, \delta), \tag{2.8}$$

where δ is a small positive number.

The second-order central differencing scheme uses

$$F^{CN}_{i+1/2} = \tfrac{1}{2}(f_{i+1} + f_i). \tag{2.9}$$

The above schemes are first order in time.

The Lax–Wendroff (LW) scheme is second order in time and space and its flux is defined as

$$F^{LW}_{i+1/2} = \frac{1}{2}(f_{i+1} + f_i) - \frac{\lambda}{2} a^2_{i+1/2}\, \Delta_{i+1/2}, \tag{2.10}$$

where

$$\lambda = \Delta t/\Delta x. \tag{2.11}$$

It is well known that the upwind scheme is too *dissipative* while the central and LW schemes are too *dispersive* in the vicinity of strong gradients.

2.2. Classification of Advanced Shock-Capturing Schemes

Currently known advanced shock-capturing schemes can be classified on the basis of:

1. The principle used to compute interface fluxes (algebraic and geometric);
2. Order of accuracy near the extrema points (ENO and TVD); and
3. Time discretization (implicit or explicit, one-step or multistep predictor-corrector).

We will follow the first classification approach, used by Zalesak [19], and organize our presentation into two classes.

Algebraic Approaches

Most of the schemes in this class, often called flux-limited schemes, are constructed in the hybrid form of added low-order, F^L, and high-order, F^H, approximations. Accordingly, the numerical flux is:

$$\begin{aligned} F_{i+1/2} &= c_{i+1/2} F^H_{i+1/2} + (1 - c_{i+1/2})\, F^L_{i+1/2} \\ &= F^L_{i+1/2} + c_{i+1/2}(F^H_{i+1/2} - F^L_{i+1/2}). \end{aligned} \tag{2.12}$$

The weight function, c, is usually computed based on flux limiters. Two such flux-limiter techniques are:

1. One-step TVD technique, representing a broad class, ranging from Roe's Superbee [1, 2], Harten [4], Chakravarthy and Osher [9], to high-order schemes of Yee [7, 20].
2. Predictor–corrector FCT technique of Boris *et al.* [22, 23], Zalesak [12, 24], and McDonald and Ambrosiano [13].

Geometric Approaches

In geometric approach, attempts are made to reconstruct dependent variable, u, within each control volume, subject to certain monotonic constraints. These constraints give the variable u at both sides of interface, $u_{i+1/2,L}$ and $u_{i+1/2,R}$. The interface flux is then computed using an exact or approximate Riemann solver. The best representative schemes in this class are: Godunov [25], van Leer's MUSCL [14], Colella and Woodward's PPM [18], and Harten and Osher's ENO [10, 11].

As will be seen, the above subdivisions are not really distinct, as several algebraic schemes can have geometric interpretations. Likewise, some geometric schemes can be derived from algebraic manipulations.

In the following subsections, brief descriptions of TVD and FCT techniques of algebraic approach and MUSCL, ENO, and PPM techniques of geometric approach are given. Due to space limitations, we will present only key features of the schemes. For more details on TVD and MUSCL type schemes, interested readers should refer to Helen Yee's excellent reviews [7, 20] of advanced differencing schemes and the original papers.

2.3. Algebraic Approach

The key to the success of the algebraic approach is in properly computing $c_{i+1/2}$ so that the solution from the numerical flux in Eq. (2.12) will satisfy certain desired properties. One such property is called total variation diminishing (TVD) introduced by Harten [6] to develop oscillation-free-schemes. He derived a set of sufficient conditions which are very useful in checking or constructing second-order TVD schemes. The scheme satisfying the TVD requirement has the property that it can prevent the total variation of the numerical approximations from increasing. The main property of a TVD scheme is that, unlike a monotone scheme (such as upwind), it can be second-order accurate and is oscillation-free across discontinuities.

The common feature of all TVD schemes is that even the high-order accurate schemes reduce to first order at local extrema. Recently, some attempts at improving this shortcoming have been reported by Harten *et al.* [10, 11] in ENO (discussed below), by Shu [26] in TVB (total variation bounded), and by Shu and Osher [27, 28] in numerical flux-based ENO.

The fundamental principle of constructing a TVD scheme is to combine low and high order fluxes so that limiters are imposed on the higher order fluxes to prevent formation of

local extrema. In the following, we give a brief description of selected, representative TVD schemes.

Second-Order TVD Scheme of Roe and Sweby

The scheme of Roe and Sweby [1–3] is a combination of first-order upwind and Lax–Windroff schemes. In terms of c in Eq. (2.12), it is defined as:

$$c_{i+1/2} = \phi(r) \tag{2.13}$$

so that

$$F_{i+1/2} = F^{\mathrm{UP}}_{i+1/2} + \phi(r)(F^{\mathrm{LW}}_{i+1/2} - F^{\mathrm{UP}}_{i+1/2}), \tag{2.14}$$

where

$$r = \frac{(|a_{i+1/2-\sigma}| - \lambda a^2_{i+1/2-\sigma})\,\Delta_{i+1/2-\sigma}}{(|a_{i+1/2}| - \lambda a^2_{i+1/2})\,\Delta_{i+1/2}},$$
$$\sigma = \mathrm{sign}(a_{i+1/2}) \tag{2.15}$$

and $\phi(r)$ is called a limiter function.

It can be seen that the classical schemes can be recovered by setting

$$\begin{aligned} &\phi(r) = 0, && \text{upwind scheme (2.5)},\\ &\phi(r) = 1, && \text{Lax–Wendroff scheme (2.10)},\\ &\phi(r) = r, && \text{Warming–Beam scheme}. \end{aligned} \tag{2.16}$$

Sweby [3] gave detailed conditions on the limiter function in order to satisfy TVD sufficient conditions. Some commonly used limiter functions are:

Minimod limiter,

$$\phi(r) = \mathrm{minimod}(1, r) \tag{2.17a}$$

Monotonic limiter,

$$\phi(r) = (r + |r|)/(1 + r) \tag{2.17b}$$

MUSCL limiter,

$$\phi(r) = \max(0, \min(2, 2r, (1 + r)/2)) \tag{2.17c}$$

Superbee limiter,

$$\phi(r) = \max(0, \min(2r, 1), \min(r, 2)), \tag{2.17d}$$

where minimod is a function defined as

$$\mathrm{minimod}(a, b) = \mathrm{sign}(a)\max(0, \min(|a|, \mathrm{sign}(a)\cdot b)). \tag{2.18}$$

Symmetric TVD Scheme of Yee, Roe, and Davis

The symmetric TVD scheme developed by Yee [6] is a generalization for Lax–Wendroff TVD schemes of Roe [1] and Davis [8]. Basically, $\phi(r)$ in Eq. (2.14) is replaced by $\phi(r^+, r^-)$,

$$F_{i+1/2} = F^{\mathrm{UP}}_{i+1/2} + \phi(r^+, r^-)(F^{\mathrm{LW}}_{i+1/2} - F^{\mathrm{UP}}_{i+1/2}), \tag{2.19}$$

where

$$r^+ = \frac{\Delta_{i+1/2+1}}{\Delta_{i+1/2}}, \qquad r^- = \frac{\Delta_{i+1/2-1}}{\Delta_{i+1/2}}. \tag{2.20}$$

The definition of two-argument limiter $\phi(r^+, r^-)$ has a similar form as single-value limiters defined by Eqs. (2.17a)–(2.17d). For example,

Minimod limiters,

$$\phi(r^+, r^-) = \mathrm{minimod}(1, r^+, r^-) \tag{2.21a}$$

$$\phi(r^+, r^-) = \mathrm{minimod}(1, r^+) + \mathrm{minimod}(1, r^-) - 1; \tag{2.21b}$$

MUSCL limiter,

$$\phi(r^+, r^-) = \max(0, \min(2, 2r^+, 2r^-, \tfrac{1}{2}(r^+ + r^-))). \tag{2.21c}$$

An alternative principle to obtain two-parameter limiters is to use any limiter of Eqs. (2.17a)–(2.17d) in conjunction with

$$\phi(r^+, r^-) = \phi(r^+) + \phi(r^-) - a, \tag{2.22}$$

where constant a may be either 1 (for minimod) or 2 (for the others).

The above "three-argument" minimod function in Eq. (2.21a) has similar form as a "two-argument" minimod defined by Eq. (2.18). Here, it is equal to: (a) the smallest number in absolute value if the list of argument is of the same sign; or (b) zero if any argument is of the opposite sign.

One-Parameter Family TVD Scheme of Chakravarthy and Osher

Instead of using the Lax–Wendroff scheme for the high-order flux in Eq. (2.12), the TVD scheme of Chakravarthy and Osher uses a second-order central difference scheme. It can be verified that the original formula of the scheme can be simplified to

$$F^{\mathrm{CO}}_{i+1/2} = F^{\mathrm{UP}}_{i+1/2} + \phi(r)[F^{\mathrm{CN}}_{i+1/2} - F^{\mathrm{UP}}_{i+1/2}]. \tag{2.23}$$

The ratio r is still defined as

$$r=\frac{a_{i+1/2-\sigma}\cdot \Delta_{i+1/2-\sigma}}{a_{i+1/2}\cdot \Delta_{i+1/2}} \tag{2.24}$$

and the limiter function $\phi(r)$ is

$$\phi(r)=\frac{3-\eta}{4}\,\text{minimod}\left(\frac{r}{\omega},1\right)+\frac{1+\eta}{4}\,\text{minimod}(1,r\omega), \tag{2.25}$$

where ω is a compressive parameter defined as

$$1\leqslant\omega\leqslant\frac{3-\eta}{1-\eta}. \tag{2.26}$$

The spatial accuracy of the scheme is controlled by the parameter η, which may take one of the following values:

$\eta=-1$	fully upwind scheme
$\eta=-\frac{1}{3}$	no name
$\eta=0$	Fromm scheme
$\eta=\frac{1}{3}$	third-order upwind-biased scheme
$\eta=\frac{1}{2}$	second-order scheme
$\eta=1$	central difference scheme.

(2.27)

The above flux is first order accurate in time. However, it is the only algebraic scheme whose higher order component in space is greater than second order. One way to obtain second-order time discretization is to replace the forward Euler time-discretization by some linear multi-step method such as the Runge–Kutta-type time discretization. For example, we can obtain

$$u_i^{n+1/2}=u_i^n-\frac{\Delta x}{2\Delta t}\left[F^n_{i+1/2}-F^n_{i-1/2}\right] \tag{2.28a}$$

$$u_i^{n+1}=u_i^n-\frac{\Delta x}{\Delta t}\left[F^{n+1/2}_{i+1/2}-F^{n+1/2}_{i-1/2}\right]. \tag{2.28b}$$

Upwind TVD Scheme of Harten and Yee

Harten [4] observed that the first-order solution applied to the equation

$$u_t+f_x=-\Delta x(\beta u_x)_x \tag{2.29}$$

results in a second-order accurate approximation to Eq. (2.1), where

$$\beta_{i+1/2}=\tfrac{1}{2}\left[\psi(a_{i+1/2})-\lambda a^2_{i+1/2}\right]. \tag{2.30}$$

He proposed to solve a modified flux equation of

$$u_t+(f+g)_x=0 \tag{2.31}$$

by an upwind scheme with $g(x)$ selected in such a way that the resulting scheme is a second-order TVD for Eq. (2.1). Harten and Yee [7] proposed the function $g(x)$ as

$$g_{i+1/2}=\Delta_{i+1/2} \tag{2.32}$$

and

$$\gamma_{i+1/2}=\beta_{i+1/2}\begin{cases}\dfrac{(g_{i+1}-g_i)}{\Delta_{i+1/2}} & \text{if } \Delta_{i+1/2}\neq 0\\ 0 & \text{if } \Delta_{i+1/2}=0,\end{cases} \tag{2.33}$$

so that

$$F_{i+1/2}=F^{\text{UP}}_{i+1/2}+\frac{\phi(r^+)+\phi(r^-)}{2}\left(F^{\text{LW}}_{i+1/2}-F^{\text{UP}}_{i+1/2}\right)-\frac{1}{2}\left[\psi(a_{i+1/2}+\gamma_{i+1/2})-\psi(a_{i+1/2})\right]\Delta_{i+1/2}, \tag{2.34}$$

where r^+ and r^- are defined in Eq. (2.20).

Comparing Eq. (2.34) with Eq. (2.14), one can see that $\phi(r)$, which is upwind weighted limiter function, has now been replaced by a central-type limiter (in which no direction of characteristic velocity is involved). $F_{i+1/2}$ now contains additional terms proportional to $\Delta_{i+1/2}$. Limiter functions (2.17a)–(2.17d) can be equally applied to $\phi(r^+)$ and $\phi(r^-)$.

Flux-Splitting TVD Scheme of Liou

The constructions of the TVD scheme of Liou [29] is somewhat similar to that of Harten and Yee's symmetric TVD scheme. The flux is, however, split as

$$f_i=f_i^+ +f_i^-, \tag{2.35}$$

where

$$f^+_{i+1}=f(a^+_{i+1}),\qquad f^-_{i+1}=f(a^-_{i+1}) \tag{2.36a}$$

$$a^+_{i+1}=\max(a_{i+1},0),\qquad a^-_{i+1}=\min(0,a_{i+1}). \tag{2.36b}$$

The upwind flux in the flux splitting notation is

$$F^{\text{UP}}_{i+1/2}=f_i^+ +f^-_{i+1} \tag{2.37}$$

and Lax–Wendroff flux is

$$F^{LW}_{i+1/2}=\frac{1}{2}(f_{i+1}+f_i)-\frac{\lambda}{2}a_{i+1/2}(f_{i+1}-f_i). \quad (2.38)$$

As a result, Liou's TVD flux can be written in a form similar to Eq. (2.34),

$$\begin{aligned}F_{i+1/2}=&F^{UP}_{i+1/2}+\tfrac{1}{2}[\phi_i(r^+)+\phi_{i+1}(r^-)]\\&\times[F^{LW}_{i+1/2}-F^{UP}_{i+1/2}]+\tfrac{1}{2}[\phi_i(r^+)-\phi_{i+1}(r^-)]\\&\times[\Delta^+ f_i-\lambda a_{i+1/2}\Delta^+ f^*],\end{aligned} \quad (2.39)$$

where

$$r^+=\frac{\Delta^- f^+}{\Delta^+ f^+},\quad r^-=\frac{\Delta^+ f^-}{\Delta^- f^-},\quad \Delta^+=(\,)_{i+1}-(\,)_i$$
$$\Delta^-=(\,)_i-(\,)_{i-1},\quad f^*=f^+-f^-. \quad (2.40)$$

The limiter functions defined in Eq. (2.17) can be used. The advantage of using flux-splitting is that it satisfies entropy inequality and is thereby capable of selecting a physically admissible solution. A contact discontinuity, however, will be smeared over a large extent.

FCT Scheme of Boris and Book

The flux corrected transport (FCT) scheme was originally developed by Boris and Book [22, 23], and later extended by Zalesak [12]. In the sense of preserving monotonicity of the solution, FCT is one kind of TVD scheme. The difference is that the TVD schemes discussed above are of one step, while the FCT is of two steps. The two-step FCT is basically a hybrid scheme consisting of a combined first- and high-order schemes. It computes a provisional update from a first-order scheme, and then filters the high-order correction by the use of flux limiters to prevent the occurrence of new extrema. Thus, in a region where the variables vary smoothly, the high-order scheme is employed. In a region where the variables vary abruptly, the low-order scheme is favored.

Formally, the FCT procedure is as follows [12]:

1. Compute low order flux $F^{L}_{i+1/2}$;
2. Compute high-order flux $F^{H}_{i+1/2}$;
3. Define the antidiffusive flux;

$$A_{i+1/2}=F^{H}_{i+1/2}-F^{L}_{i+1/2}; \quad (2.41)$$

4. Compute the updated low-order solution,

$$u^{td}=u^n-\lambda(F^{L}_{i+1/2}-F^{L}_{i+1/2}); \quad (2.42)$$

5. Limit or correct $A_{i+1/2}$ as

$$A^c_{i+1/2}=c_{i+1/2}A_{i+1/2}; \quad (2.43)$$

6. Apply the limited antidiffusive flux,

$$u^{n+1}_i=u^{td}_i-\lambda(A^c_{i+1/2}-A^c_{i-1/2}). \quad (2.44)$$

In the above, Step 5 is critical. It ensures that u^{n+1}, computed in Step 6, does not have any new extremum (as compared to those which exist in u^{td} and u^n). The definition of high-order flux in Step 2 is also important for final accuracy of the solution.

The original algorithm for flux-limiting was given by Boris and Book [22, 23]. The higher order flux is by Lax–Wendroff scheme and the low-order flux is by upwind. They defined the antidiffusive flux as

$$\begin{aligned}A^c_{i+1/2}=S\cdot\max\Bigg\{0,\min\Bigg[&|A_{i+1/2}|,\\&\frac{S(u^{td}_{i+2}-u^{td}_{i+1})}{\lambda},\frac{S(u^{td}_i-u^{td}_{i-1})}{\lambda}\Bigg]\Bigg\},\\S=&\operatorname{sign}(A_{i+1/2}).\end{aligned} \quad (2.45)$$

It is noticed that the difference between the limiting procedures of TVD and FCT schemes lies in that FCT schemes use an updated value, whereas TVD schemes use the old time level value. That is the reason the FCT scheme is of two steps.

FCT Scheme of Zalesak

In Zalesak's version of the FCT [12], the coefficient $c_{i+1/2}$ is obtained from a complicated recipe which is omitted here. The interested reader should refer to the original paper for the details. The high-order scheme is by the fourth, sixth, and eighth order central difference.

FCT Scheme of McDonald and Ambrosiano

McDonald and Ambrosiano [13] found that Zalesak's FCT scheme, employing a donor cell algorithm as the first part and a flux-limited spatially centered high-order correction, produced some pathological results. The worst of these included the formation of "staircases" on a steepening slope. In another case, a non-physical shock, arising out of an expansion region, was produced. They improved the FCT scheme through the use of totally one-sided differences.

The high-order upwind for flux function is

$$F^{H}_{i+1/2}=\begin{cases}\frac{3}{2}f_i-\frac{1}{2}f_{i-1} & \text{if } a_{i+1/2}\geqslant 0\\ \frac{3}{2}f_{i+2}-\frac{1}{2}f_{i+1} & \text{if } a_{i+1/2}<0.\end{cases} \quad (2.46)$$

The low-order scheme is the first-order upwind, and the antidiffusive flux is the same as Eq. (2.45).

2.4. Geometrically Formulated Schemes

The notion of algebraic and geometric approaches was introduced by Goodman and LeVeque [15]. The former scheme is to algebraically enforce some constraints on the problem (such as on flux). Thus, algebraic relations are derived which guarantee certain desirable properties. Geometric approach, on the other hand, attempts to:

1. Interpolate the dependent variable within the control volume including cell interface (where a discontinuity may occur); and

2. Compute the interface fluxes using exact or approximate Riemann solver or by tracing characteristics to the cell interface.

The detailed procedure of a geometric approach can be divided into the following steps:

1. Compute profiles of the dependent variable in each zone by interpolating slopes or curvatures at the center of zones, subject to certain monotonicity constraints. This gives rise to a global distribution of the dependent variable which is piecewise constant (Godunov), linear (MUSCL), or parabolic (PPM) in each zone with jump discontinuities $(u_{i+1/2,\mathrm{L}}, u_{i+1/2,\mathrm{R}})$ at the edge of zones.

2. Compute $u^n_{i+1/2}$, the solution of the old time at the edge of zones, by solving the Riemann problems which resolve the jump discontinuities at the edge of the zones (with $u_{i+1/2,\mathrm{L}}$, and $u_{i+1/2,\mathrm{R}}$).

3. Compute $u^{n+1/2}_{i+1/2}$, an approximation of the solution at the edge of the zone at the half time step, by approximately tracing the characteristics and solving the difference approximation to the characteristics equations, or by transporting the distributed profile.

4. Compute time-averaged value of $F^{n+1/2}_{i+1/2}$.

5. Use the above flux to calculate the dependent quantities:

$$u_i^{n+1} = u_i^n - \lambda(F^{n+1/2}_{i+1/2} - F^{n+1/2}_{i-1/2}). \tag{2.47}$$

Different schemes use different methods to evaluate $u_{i+1/2}$ or $F_{i+1/2}$. In the following, we will discuss them individually.

MUSCL Scheme of van Leer

Van Leer [14] observed that one can obtain spatially higher-order accuracy in the original Godunov scheme by replacing piecewise constant data of the Riemann problem with piecewise linear data. In addition, he replaced an exact Riemann solver by Roe's approximate Riemann solver [30]. In his MUSCL (monotonic upwind scheme for conservation laws) scheme, the value of the dependent variable at the grid cell interface is obtained through the following slope (minimod) limiters [30]:

$$u^{\mathrm{R}}_{i+1/2} = u_{i+1} - \tfrac{1}{4}\left[(1-\eta)\,\Delta^{\sim}_{i+3/2} + (1+\eta)\,\Delta^{\approx}_{i+1/2}\right] \tag{2.48a}$$

$$u^{\mathrm{L}}_{i+1/2} = u_i + \tfrac{1}{4}\left[(1-\eta)\,\Delta^{\approx}_{i-1/2} + (1+\eta)\,\Delta^{\sim}_{i+1/2}\right] \tag{2.48b}$$

$$\Delta^{\sim}_{i+1/2} = \mathrm{minimod}(\Delta_{i+1/2}, \omega\Delta_{i-1/2}) \tag{2.48c}$$

$$\Delta^{\approx}_{i+1/2} = \mathrm{minimod}(\Delta_{i+1/2}, \omega\Delta_{i+3/2}). \tag{2.48d}$$

The spatial order of accuracy is determined by Eq. (2.26), and Roe's approximate Riemann solver gives

$$F(u^n_{i+1/2}) = \frac{1}{2}\left[f(u_{i+1/2,\mathrm{R}}) + f(u_{i+1/2,\mathrm{L}}) - \left|\frac{f(u_{i+1/2,\mathrm{R}}) - f(u_{i+1/2,\mathrm{L}})}{(u_{i+1/2,\mathrm{R}} - u_{i+1/2,\mathrm{L}})}\right| \times (u_{i+1/2,\mathrm{R}} - u_{i+1/2,\mathrm{L}})\right]. \tag{2.49}$$

To obtain a second-order time-discretization (in addition to the above higher order spatial discretization) one can replace the forward Euler time-discretization (2.47) by some linear multiple step method (see Eq. (2.28)) or by the Runge–Kutta-type of discretization.

MUSCL Scheme of Goodman and LeVeque

Goodman and LeVeque [15] derived a second-order accurate TVD scheme using a geometric approach in line with van Leer's work. In addition to choosing the slope properly in the piecewise linear approximation for dependent variable, the scheme is accomplished by approximating the flux function f to be piecewise linear. The purpose of the later approximation is that the modified equation with piecewise linear initial data can be efficiently solved analytically. It also has the advantage of ease in getting $F(u^{n+1}_{i+1/2})$ through characteristic tracing. Actually, for a linear problem it agrees with one of the flux-limiter methods of the Roe–Sweby TVD scheme. No such agreement exists for the nonlinear problem.

A piecewise linear function of u denoted by v in the region $x_{i-1/2}$ and $x_{i+1/2}$is constructed as

$$v(x, t^n) = u_i^n + S_i^n \frac{x - x_i}{\Delta x}, \tag{2.50}$$

where S_i^n is determined from some limiter functions, for example,

$$S_i^n = \mathrm{minimod}(\Delta_{i+1/2}, \Delta_{i-1/2}); \tag{2.51}$$

$u^n_{i+1/2,\mathrm{R}}$ and $u^n_{i+1/2,\mathrm{L}}$, at interface, are calculated using Eq. (2.50),

$$u^n_{i+1/2,\mathrm{R}} = u^n_{i+1} - \tfrac{1}{2} S^n_{i+1}, \qquad u^n_{i+1/2,\mathrm{L}} = u^n_i + \tfrac{1}{2} S^n_i. \tag{2.52}$$

Assume a piecewise linear function of flux on u (denoted by g), with a slope g'_i,

$$g'_i = \begin{cases} \dfrac{f(u_{i+1/2,\mathrm{R}}) - f(u_{i+1/2,\mathrm{L}})}{(u_{i+1/2,\mathrm{R}} - u_{i+1/2,\mathrm{L}})} & \text{if } S^n_i \neq 0 \\ f'(u_i) & \text{if } S^n_i = 0 \end{cases} \tag{2.53}$$

then the flux is

$$F_{i+1/2} = \frac{1}{\Delta t}\int_{t^n}^{t^{n+1}} g[v(x_{i+1/2}, t)]\, dt = \begin{cases} f(u_{i+1/2,\mathrm{R}}) - \tfrac{1}{2}\lambda S^n_i (g'_i)^2 & \text{if } f' > 0 \\ f(u_{i+1/2,\mathrm{L}}) - \tfrac{1}{2}\lambda S^n_i (g'_{i+1})^2 & \text{if } f' < 0. \end{cases} \tag{2.54}$$

MUSCL Scheme of Colella

Colella [17] used a two-step algorithm to calculate the slope of u in each zone. The first guess is a monotonized central difference algorithm discussed by van Leer [14]:

$$\delta_i u_i = 2\ \mathrm{minimod}(\Delta_{i+1/2}, \Delta_{i-1/2}) \tag{2.55}$$

$$\delta_f u_i = \min\left(\frac{(\Delta_{i+1/2} + \Delta_{i-1/2})}{2}, \delta_i u_i\right) \times \mathrm{sign}(\Delta_{i+1/2} + \Delta_{i-1/2}). \tag{2.56}$$

Finally, he calculated S^n_i by differencing the values at two points on either side of i obtained by using $\delta_f u$ as the slope:

$$S^n_i = \min[\tfrac{2}{3}|\Delta_{i+1/2} + \Delta_{i-1/2} - \tfrac{1}{4}(\delta_f u_{i+1} - \delta_f u_i)|, \delta_f u_i] \times \mathrm{sign}(\Delta_{i+1/2} + \Delta_{i-1/2}). \tag{2.57}$$

In the case where the minima in Eq. (2.55)–(2.57) are obtained in the first argument, one obtains

$$S^n_i = \tfrac{2}{3}(u_{i+1} - u_{i-1}) - \tfrac{1}{12}(u_{i+2} - u_{i-2}). \tag{2.58}$$

This is a fourth-order finite difference approximation to du/dx. Thus, it is well behaved in the regions where the solution is smooth.

MUSCL Scheme of Davis

In Davis' MUSCL scheme [16], the piecewise-linear interpolation of u is assumed, and the slope of the profile is determined from a minimod function of:

$$S^n_i = \begin{cases} \mathrm{sign}(\Delta_{i+1/2} + \Delta_{i-1/2}) \times \min(\tfrac{1}{2}|\Delta_{i+1/2} + \Delta_{i-1/2}|, 2|\Delta_{i+1/2}|, 2|\Delta_{i-1/2}|) \\ \qquad \text{if } \Delta_{i+1/2} \cdot \Delta_{i-1/2} > 0 \\ 0, \quad \text{otherwise.} \end{cases} \tag{2.59}$$

It is basically the original van Leer's MUSCL limiter [14] in Eq. (2.56). Instead of Roe's approximate Riemann solver, as used by van Leer [30], Davis used the approximate Riemann solution of Harten and Lax [31]. It contains only one intermediate state for any hyperbolic conservation law. The construction of this approximate solution assumes that the bounds on the smallest and largest signal velocities (a_{L} and a_{R}) in the exact Riemann solution are available a priori. The flux on a cell face by this approximation is then given by

$$F_{i+1/2} = \begin{cases} f_{\mathrm{L}} & \text{when } 0 < a_{\mathrm{L}} \\ \dfrac{-a_{\mathrm{L}}}{a_{\mathrm{R}} - a_{\mathrm{L}}} f_{\mathrm{R}} + \dfrac{a_{\mathrm{L}}}{a_{\mathrm{R}} - a_{\mathrm{L}}} f_{\mathrm{L}} + \dfrac{a_{\mathrm{R}} a_{\mathrm{L}}}{a_{\mathrm{R}} - a_{\mathrm{L}}}(u_{\mathrm{R}} - u_{\mathrm{L}}) & \text{when } a_{\mathrm{L}} < 0 < a_{\mathrm{R}} \\ f_{\mathrm{R}} & \text{when } a_{\mathrm{R}} < 0. \end{cases} \tag{2.60}$$

Davis proposed that the a_{L} and a_{R} be determined as

$$a_{\mathrm{L}} = \min[\beta_1(u_{\mathrm{L}}), \beta_1(u_{\mathrm{R}})], \qquad a_{\mathrm{R}} = \max[\beta_m(u_{\mathrm{L}}), \beta_m(u_{\mathrm{R}})], \tag{2.61}$$

where β_1 and β_m are minimum and maximum characteristic speeds, respectively.

To obtain high-order accuracy in time, Davis proposed the explicit predictor–corrector scheme,

$$u^{n+1/2}_i = u^n_i - \frac{\lambda}{2}\left[f\left(u^n_i + \frac{S^n_i}{2}\right) - f\left(u^n_i - \frac{S^n_i}{2}\right)\right] \tag{2.62}$$

and

$$u^{n+1}_i = u^n_i - \lambda[F_{i+1/2}(u^{n+1/2}_{i+1/2,\mathrm{R}}, u^{n+1/2}_{i+1/2,\mathrm{L}}) - F_{i-1/2}(u^{n+1/2}_{i-1/2,\mathrm{R}}, u^{n+1/2}_{i-1/2,\mathrm{L}})], \tag{2.64}$$

where

$$F_{i+1/2}(u^{n+1/2}_{i+1/2,\mathrm{R}}, u^{n+1/2}_{i+1/2,\mathrm{L}}) = F_{i+1/2}(u^{n+1/2}_i + \tfrac{1}{2} S^n_i, u^{n+1/2}_{i+1} - \tfrac{1}{2} S^n_{i+1}). \tag{2.64}$$

The flux function $F_{i+1/2}$ is calculated based on the approximate Riemann solver (Eq. (2.49)).

ENO Scheme of Harten and Osher

Harten and Osher [10] observed that a TVD scheme, which is constructed to prevent an increase in the total variation of the numerical approximations, has at most first-order accuracy. They consequently constructed a new class of schemes which they called ENO schemes (essentially non-oscillatory). These schemes are essentially non-oscillatory, uniformly second-order accurate, and do not possess undesired clipping phenomena. Unlike TVD

Osher [27, 28] have extended the ENO construction to a numerical flux based procedure. Interested readers should refer to the original paper for details. It is expected that for linear problems both construction procedures are the same.

PPM Scheme of Colella and Woodward

The piecewise-parabolic method (PPM) due to Colella and Woodward [18] is a higher-order extension of Godunov's method of the type introduced by van Leer in his

damp the values of each local extremem at every single time step. Instead, they are allowed to occasionally accentuate local extrema.

The major disadvantage of ENO schemes is that they are more expensive than TVD schemes. This is due to the fact that ENO schemes use wider (7-point vs 5-point) finite-

rithms. The PPM scheme uses an interpolation which is piecewise continuous with u given by a parabolic profile in each zone,

$$u(x) = u_{i-1/2,\mathrm{R}} + \xi[\Delta u_i + u_{6,i}(1-\xi)], \qquad (2.69)$$

As a result, the interpolation function $u(x)$ is continuous at $x_{i+1/2}$. If the interpolation function $u(x)$ takes on the values which are not between $a_{i+1/2,\mathrm{L}}$ and $a_{i+1/2,\mathrm{R}}$, further limiting must be applied to fulfill monotonicity. The left and right state values $u_{i+1/2,\mathrm{L}}$ and $u_{i+1/2,\mathrm{R}}$ are therefore modified so that $u(x)$ is a monotonic function on each interval $(x_{i-1/2}, x_{i+1/2})$. Let

$$d_1 = u_{i+1/2,\mathrm{L}} - u_i^n \tag{2.75a}$$

$$d_2 = u_{i-1/2,\mathrm{R}} - u_i^n \tag{2.75b}$$

$$u_{i-1/2,\mathrm{R}} = u_i^n, \qquad u_{i+1/2,\mathrm{L}} = u_i^n$$
$$\text{if} \quad -d_1 \cdot d_2 \leqslant 0 \tag{2.75c}$$

$$u_{i-1/2,\mathrm{R}} = 3u_i^n - 2u_{i+1/2,\mathrm{L}}$$
$$\text{if} \quad -\tfrac{1}{2}(d_1^2 - d_2^2) > \tfrac{1}{6}(d_1 - d_2)^2 \tag{2.75d}$$

$$u_{i+1/2,\mathrm{L}} = 3u_i^n - 2u_{i-1/2,\mathrm{R}}$$
$$\text{if} \quad \tfrac{1}{2}(d_1^2 - d_2^2) > \tfrac{1}{6}(d_1 - d_2)^2. \tag{2.75e}$$

This step introduces discontinuities at the cell faces (zone edges). Finally, the cell face flux is computed as

$$f_{i+1/2} = \begin{cases} f[u_{i+1/2,\mathrm{L}}(a_{i+1/2}\,\Delta t)] & \text{if} \quad a_{i+1/2} \geqslant 0 \\ f[u_{i+1/2,\mathrm{R}}(-a_{i+1/2}\,\Delta t)] & \text{if} \quad a_{i+1/2} < 0, \end{cases} \tag{2.76}$$

where

$$u_{i+1/2,\mathrm{L}}(x) = u_{i+1/2,\mathrm{L}} - \frac{\xi}{2}\left[\Delta u_i - \left(1 - \frac{2}{3}\xi\right) u_{6,i}\right]$$
$$\text{for} \quad \xi = \frac{x - x_i}{\Delta x_i} \tag{2.77a}$$

$$u_{i+1/2,\mathrm{R}}(x) = u_{i+1/2,\mathrm{R}} + \frac{\xi}{2}\left[\Delta u_{i+1} + \left(1 - \frac{2}{3}\xi\right) u_{6,i+1}\right]$$
$$\text{for} \quad \xi = \frac{x - x_{i+1}}{\Delta x_{i+1}}. \tag{2.77b}$$

3. RESULTS AND DISCUSSIONS

In the following, we will compare the performance of various shock-capturing schemes applied to Burgers' equation. The main interest here will be on transient solution which includes formation, propagation, and collision of shocks, and expansion of discontinuities.

The well-known inviscid Burgers' equation is written as

$$u_t + \left(\frac{u^2}{2}\right)_x = 0 \tag{3.1}$$

or

$$u_t + uu_x = 0 \tag{3.2}$$

with the initial condition of

$$u(x, 0) = u_0(x). \tag{3.3}$$

The characteristic speed, as indicated in Eq. (3.2), is u. Along the characteristic trajectory,

$$\frac{dx}{dt} = u, \tag{3.4}$$

the transport property, u, is constant. Since the characteristic speed u is not a constant, but depends on the solution itself, Eq. (3.2) is a nonlinear wave equation, where each point on the wave front can propagate with a different speed. The result of changing wave speed leads to the formation of a discontinuous solution.

In some cases, Eq. (3.1) admits an analytic solution up to the time at which a shock is formed. This solution may be found as

$$u(x, t) = u_0(x - ut). \tag{3.5}$$

The solution is generated by solving the nonlinear equation (3.5) for u in terms of x and t. When a shock is formed, the solution can still be found through piecewise solution of Eq. (3.5) on both sides of the shock.

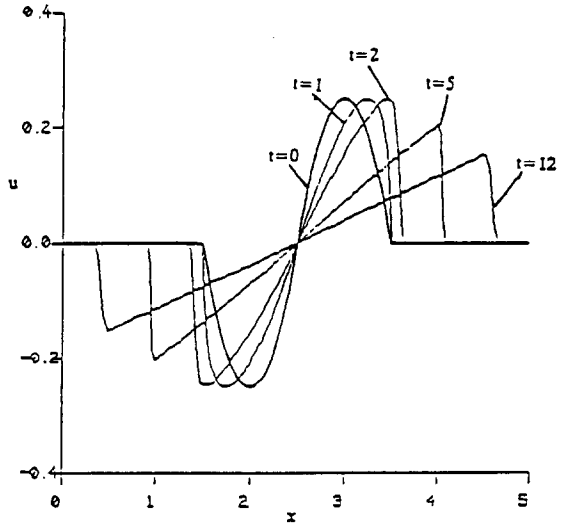

FIG. 2. Initial conditions and analytical solutions for the formation and propagation of shock.

3.1. Formation and Propagation of Shocks

The first test case considered is from McDonald and Ambrosiano [13] and represents the wave propagation of an initial parabolic profile defined as

$$\begin{aligned} y &= x - 2.5 \\ u_0(y) &= \max[0,\ y(1-y)]: \quad y \geqslant 0 \\ u_0(y) &= -u_0(y): \qquad\quad y < 0, \end{aligned} \tag{3.6}$$

where x varies from 0.0 to 5.0 and a cyclic boundary condition is applied at two ends. The initial condition at $t = 0$ and analytical solution at different time are illustrated in Fig. 2.

In the region of $3.0 \leqslant x < 3.5$ (similarly applied to $1.5 \leqslant x < 2.0$), the characteristic speed decreases (increases) with x, so that a shock tends to form. In the region $2.0 < x < 3.0$, an expansion is present. At time of $t = 1.0$, all properties along the characteristic trajectory collapse so that two shocks are formed at about $x = 3.5$ and $x = 4.5$, respectively. After that they move with a velocity of

$$u_s = \tfrac{1}{2}(u_L + u_R), \tag{3.7}$$

where u_L and u_R are the speed on both sides of the shock front. The initial parabola wave now becomes an N-wave.

Calculations were carried out on a uniform grid of 40 intervals, and time step size was chosen as $\Delta t/\Delta x = 0.4$. The corresponding CFL is 0.1. The results to be presented are at $t = 2.0$ and $t = 12.0$, which are right after formation of the shock and after a certain time of the shock propagation.

Shown in Figs. 3a are the results of TVD schemes at times 2.0 and 12.0. Since most TVD schemes are a combination of upwind and Lax–Wendroff schemes, we also display the results of both of these schemes in Fig. 3a and 3b, respectively. It is seen that the calculation with upwind scheme, as expected, is relatively dissipative, especially near the local maximum and minimum and in the shock front region.

The results obtained with the Lax–Wendroff scheme (Fig. 3b), on the other hand, show good results in the monotonic region and the ripples near the extreme at an earlier time when the solution is smooth. At a later time when the shocks form and propagate, the Lax–Wendroff scheme leads to a nonlinear instability, and the result is totally unacceptable.

The Warming–Beam scheme, shown in Fig. 3c, surprisingly gives an excellent representation in both shock and smooth solutions. It would not have been a surprise if we looked at the mathematical meaning of minimod $\phi(1, r)$. What the limiter tells us is that as long as the profile is monotonic ($r > 0$), the TVD scheme of Roe and Sweby either picks up the Warming–Beam scheme ($\phi(r) = r$) if $r < 1$ or the Lax–Wendroff scheme ($\phi(r) = 1$) if $r > 1$. In other words, the Warming–Beam scheme satisfies the TVD sufficient conditions if $1 > r > 0$ and the Lax–Wendroff scheme is TVD if $r > 1$. In the region before the local extrema, $1 > r > 0$, we expect that the TVD scheme will most likely pick up the Warming–Beam scheme, which has no spurious oscillation, and will abandon Lax–Wendroff scheme, which gives overshoots and undershoots.

Roe and Sweby's TVD scheme with a superbee limiter, as illustrated in Fig. 3d, and the upwind TVD scheme (modified flux approach of Harten and Yee) with a MUSCL limiter, illustrated in Fig. 3e, behave well in continuous and discontinuous portions of the solution. The symmetric TVD scheme with a MUSCL limiter, illustrated in Fig. 3f, does not perform well compared to Roe and Sweby's TVD scheme with a superbee limiter. One sees the ripples near the shock fronts and the slower propagation speed of the shocks. Actually, the limiting practice in the symmetric TVD scheme has no direction involved; r^+ and r^- are equally applied. This may sometimes lead to a non-physical backward propagation of dispersive ripples resulting from a sudden change in the slope. The symmetric TVD scheme, however, is much better than either the upwind or the Lax–Wendroff schemes. Chakravarthy and Osher's TVD scheme with third-order accuracy ($\eta = \frac{1}{3}$), illustrated in Fig. 3g, performs exceptionally well. The solution is relatively crisp in the expansion region. Liou's flux-splitting TVD scheme with a monotonic limiter (Fig. 3h) is a little better than the symmetric TVD scheme. Near the sonic point ($u = 0$), the numerical solution of Liou's TVD scheme is not that smooth, due to the inherent difficulty with flux splitting.

Shown in Fig. 3i and j are the results from Zalesak's FCT limiting algorithm for a second-order central difference in space and time, an eighth-order in space and fourth-order Runge-Kutta in time. Early in time, when the solution is still smooth, both schemes show remarkable accuracy and perform better than TVD schemes. Later in time, however, the solutions show wiggles all over the place (even though they are very close to the exact solution). Careful examination of both figures reveals that there are "staircases" near the sonic point and upstream of the shocks. This pathology is not a result of nonlinear propagation, but is associated with the shape of the profile. The same behavior has also been observed when a semi-elliptic profile was transported by linear advection [13]. Because the slope of the function changes continuously from a finite value towards an infinite value (near the shock), there is a point in the curve from which the centered finite-difference derivative begins to produce Gribbs oscillation. When these are clipped by the flux-limiter, the staircase appears. Using the upwind FCT of McDonald and Ambrosiano, which is second-order accurate in space and time, the staircase disappears (see Fig. 3k), and the overall accuracy is comparable to TVD schemes. The result of the second-order centered difference scheme with Boris and Book's limiting algorithm, shown in

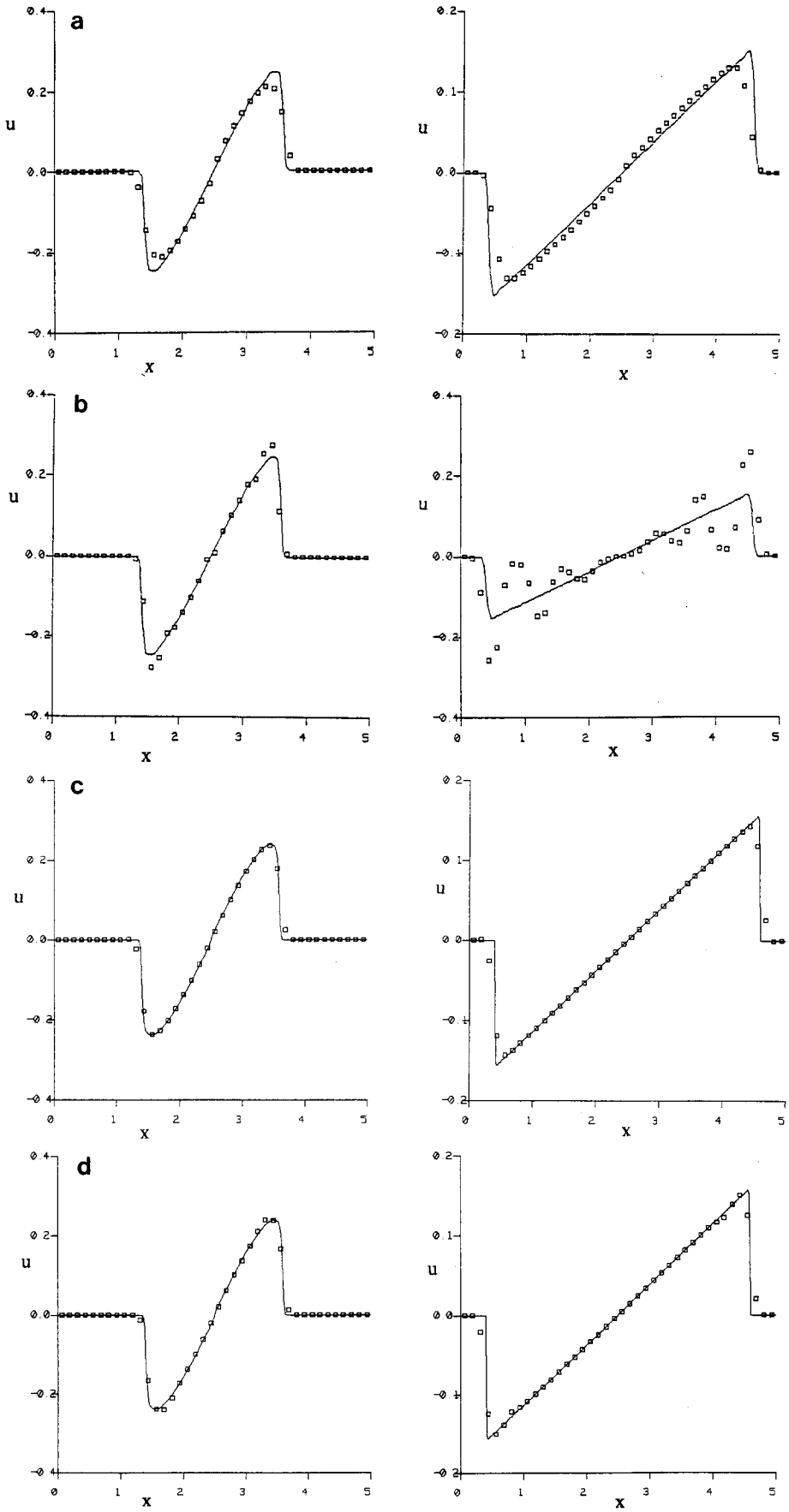

FIG. 3. TVD schemes at times 2.0 and 12.0: (a) first-order upwind; (b) Lax–Wendroff; (c) Warming–Beam; (d) superbee limiter, Roe and Sweby's TVD; (e) MUSCL limiter, upwind TVD; (f) MUSCL limiter, symmetric TVD; (g) third-order scheme, Chakravarthy and Osher's TVD; (h) monotonic limiter, Liou's TVD; (i) second-order FCT of Zalesak; (j) eighth-order FCT of Zalesak; (k) second-order upwind FCT of McDonald and Ambrosiano; (l) second-order FCT of Boris and Book; (m) MUSCL of Goodman and LeVeque; (n) PPM of Colella and Woodward; (o) ENO of Harten and Osher; (p) FNO of Harten and Osher.

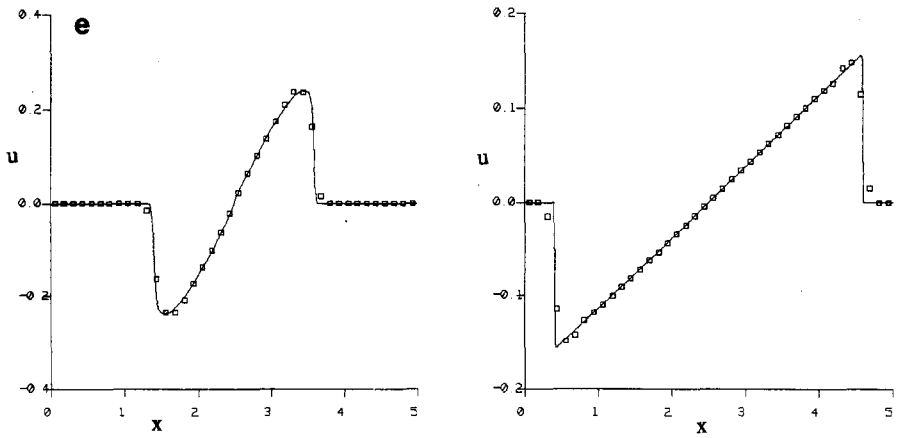
e
u
x

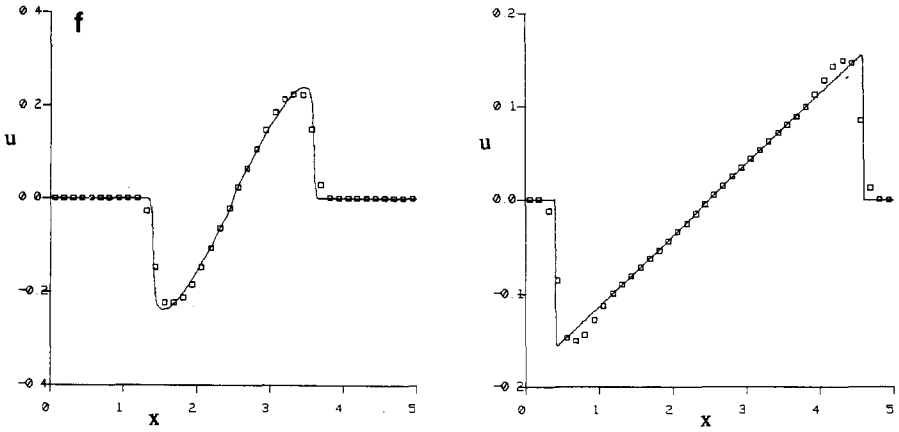
f
u
x

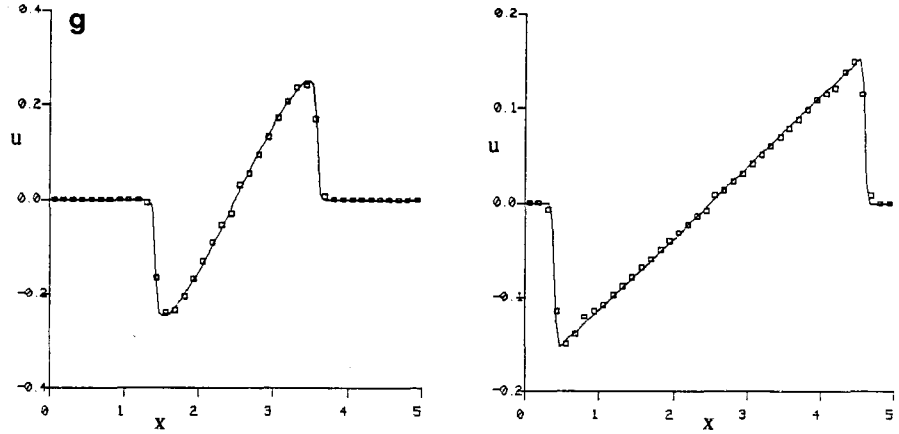
g
u
x

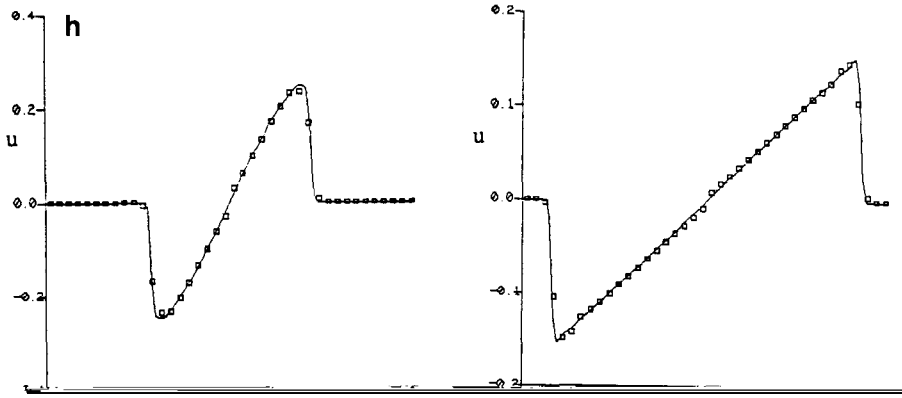
h
u
x

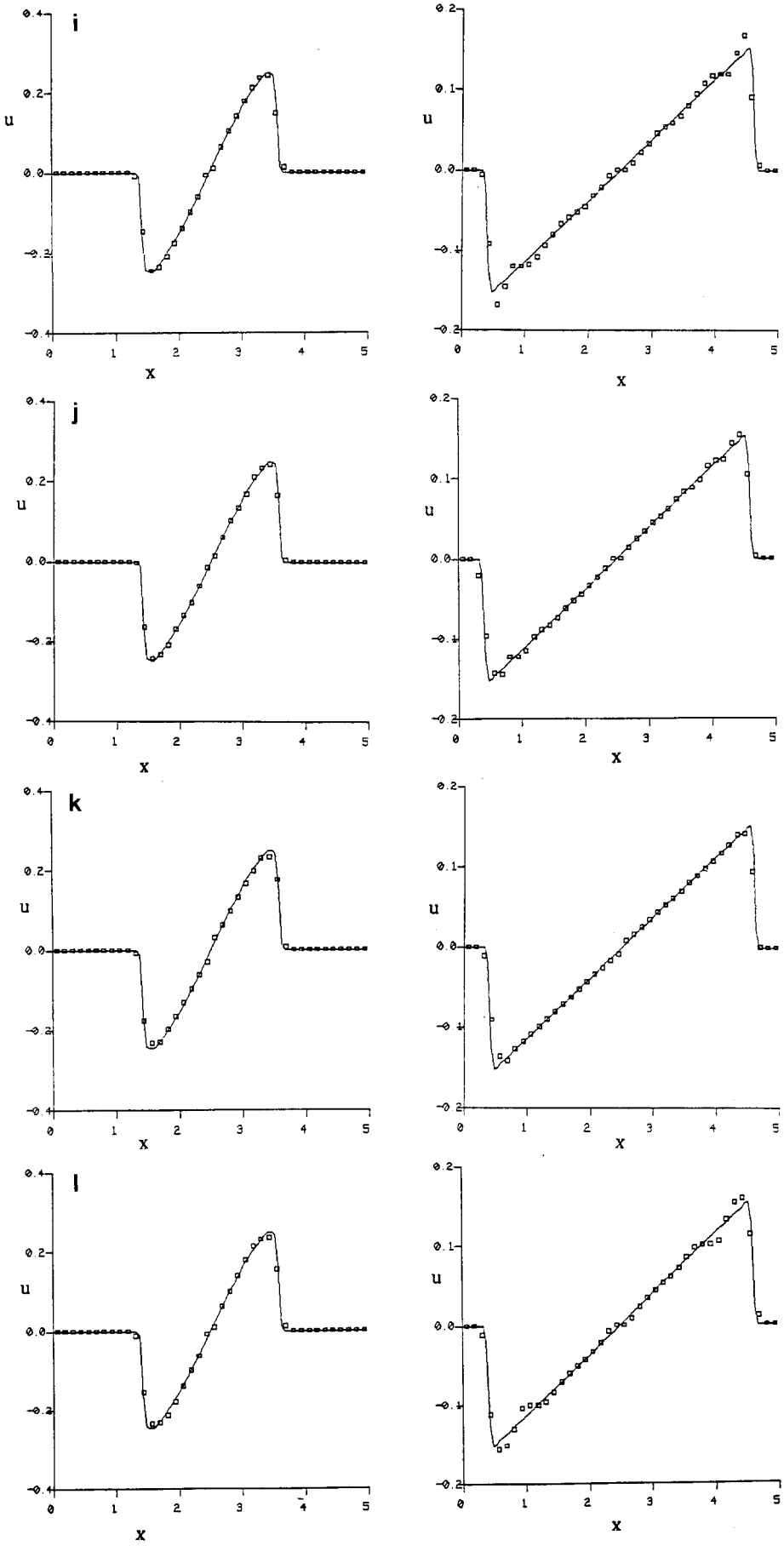

FIG. 3—*Continued*

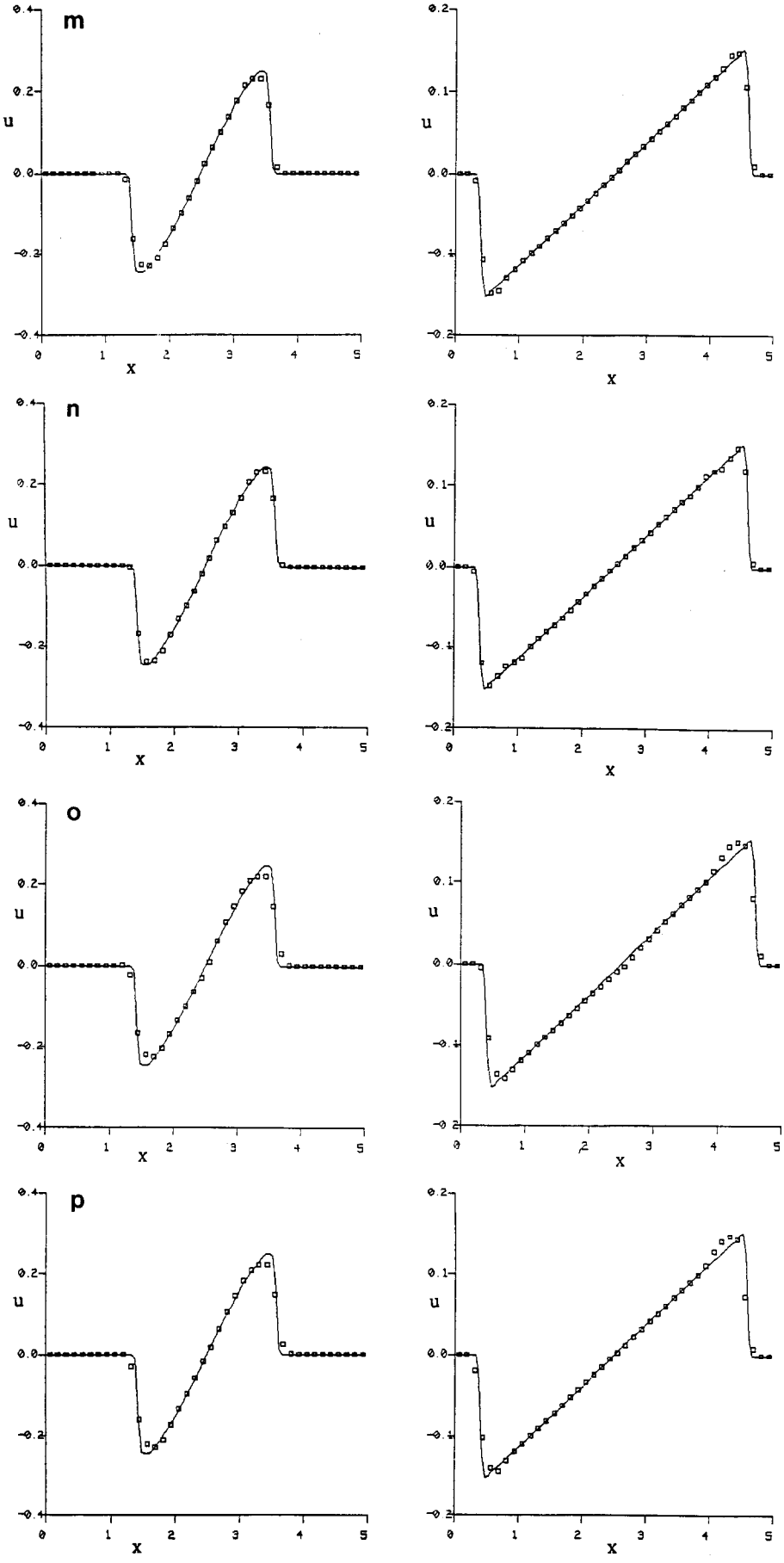

FIG. 3—*Continued*

Fig. 3l, is almost the same as the one with Zalesak's limiting algorithm, Fig. 3i.

The MUSCL scheme of Goodman and LeVeque (Fig. 3m) gives excellent results in both smooth and discontinuous regions of the solution. It is comparable with TVD schemes. The PPM scheme, shown in Fig. 3n, which assumes a parabolic distribution, indeed performs better than MUSCL schemes. It is especially obvious near the local extrema, both in the expansion and the shock regions. On the other hand, ENO and FNO schemes (Fig. 3o and 3p) are more diffusive. Their solutions also display a ripple upstream of the shock. This gehavior is similar to that of the symmetric TVD scheme. FNO, as claimed by Harten and Osher [10], is better than ENO, especially near the expansion and sonic points.

3.2. Expansion of Discontinuities and Collision of Shocks

The second test case, we propose for Burgers' equation, is the propagation of initial square waves in different directions. This test case contains both expansion of discontinuities and collision of shocks. The initial profile is specified as

$$u(x,0)=\begin{cases}1.0 & 2.0>x>0.2\\ -0.5 & 3.0>x>2.0\\ -1.0 & 4.8>x>3.0\\ 0 & \text{otherwise}\end{cases} \tag{3.8}$$

and is shown with the solid line ($t=0$) on Fig. 4. Two shocks are initially located at $x=2$ (right moving shock) and at $x=3$ (left moving shock). Additionally, two steep expansion discontinuities are located at $x=0.2$ (expanding to the right) and at $x=4.8$ (expanding to the left).

The time evolution of the initial waves is also shown in Fig. 4. During the earlier time, at $x=0.2$ and 4.8, two expansion fans appear. At $x=2.0$ the shock with positive speed (u) moves to the right; and at $x=3.0$ the shock with negative speed (u) moves to the left. At time $=1.0$, two shocks meet and collide, and then become a single one, propagating to the left.

In the numerical computations, we still use 40 grids and keep $\Delta t/\Delta x=0.4$, so that the corresponding CFL is 0.4. The numerical results are presented at the time of $t=0.75$ when the shocks are about to meet and at $t=2.0$ when the two shocks collapse and form a single one.

The upwind scheme result, shown in Fig. 5a, is so diffusive that the shocks and expansion fans are smeared out. The Lax–Wendroff scheme (Fig. 5b) shows overshoots in the front of the shock where r is less than zero. Thus this scheme violates the TVD criterion. The Warming–Beam scheme (Fig. 5c), on the other hand, gives ripples in the expansion region instead in the front of the shock. The reason is because r is larger than 1 in the expansion part and

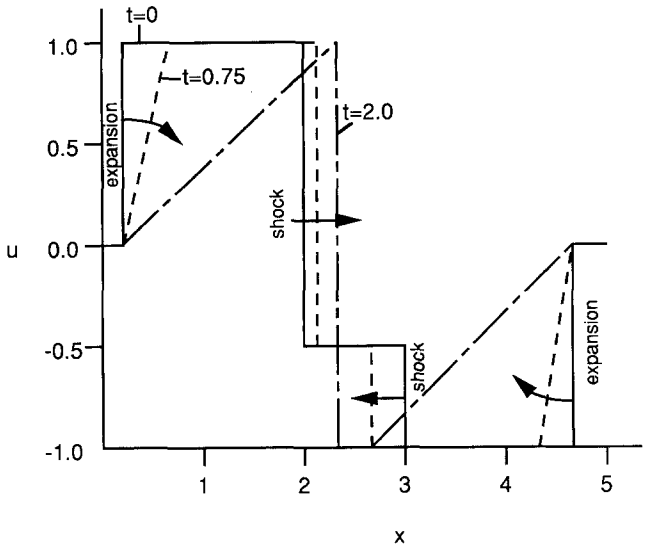

FIG. 4. Initial conditions and analytical solutions for the case of expanding discontinuities and colliding shocks.

TVD requires using the Lax–Wendroff scheme. The superbee limiter of Roe and Sweby's TVD scheme (Fig. 5d) again gives excellent results in the expansion and in the shock front regions.

From Figs. 5e to g, we present the velocities from the same minimod type of limiter but different schemes: Roe and Sweby's TVD (Fig. 5e), the upwind TVD (Fig. 5f), and the symmetric TVD (Fig. 5g). For Roe and Sweby's TVD method, one would expect the scheme to use the Lax–Wendroff algorithm in the expansion region and the Warming–Beam in front of the shock. Comparison of Fig. 5e with Fig. 5b and c proves the above point. Compared with the superbee limiter, the minimod limiter is more diffusive. The upwind TVD scheme is as good as Roe and Sweby's TVD scheme. The symmetric TVD scheme, with the same minimod limiter, is more diffusive than Roe and Sweby's TVD scheme. In comparing the two schemes, one finds that the difference is in the $\phi(r)$ and $\phi(r^+, r^-)$ limiters:

$$\begin{aligned}\phi(r)&=\text{minimod}(1,r)\\ \phi(r^+,r^-)&=\text{minimod}(1,r^+)+\text{minimod}(1,r^-)-1.\end{aligned} \tag{3.9}$$

We see that $\phi(r^+, r^-)\leqslant\phi(r)$; therefore, the symmetric TVD scheme contains a larger amount of dissipation.

The one-parameter family TVD scheme of Chakravarthy and Osher with $\eta=0$, i.e., Fromm's scheme (see Fig. 5h) is relatively compressive and gives good representation of discontinuities. It does not perform well in the expansion region. The flux-splitting TVD of Liou with minimod (not shown here) is similar to Roe and Sweby's TVD with the same limiter.

Zalesak's second-order scheme (Fig. 5i) now shows

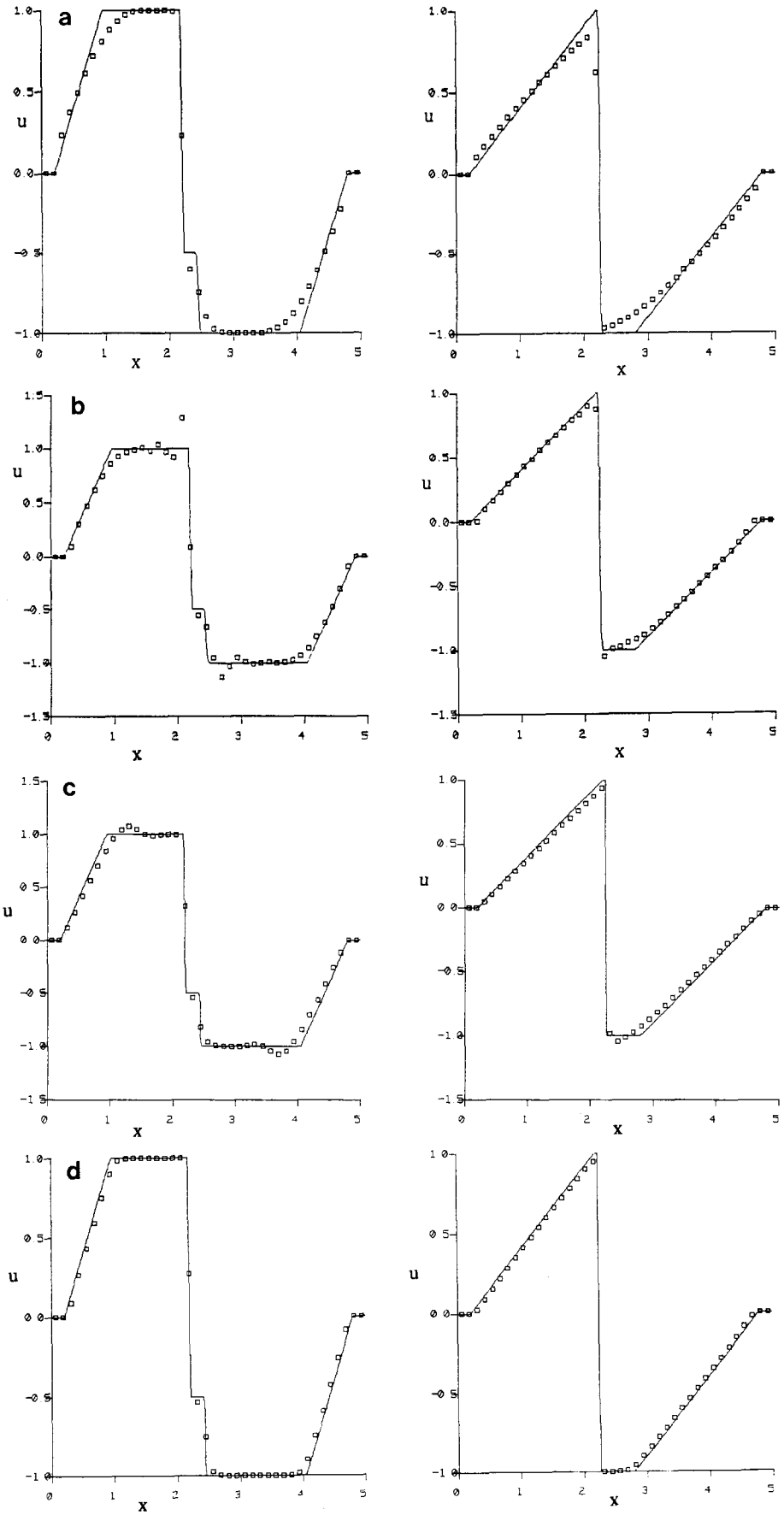

FIG. 5. Numerical results for time 0.75 when the shocks are about to meet and for time 2.0 when the two shocks collapse and form a single one: (a) first-order upwind; (b) Lax–Wendroff; (c) Warming-Beam; (d) superbee limiter, Roe and Sweby's TVD; (e) minimod limiter, Roe and Sweby's TVD; (f) minimod limiter, upwind TVD; (g) minimod limiter, symmetric TVD; (h) Fromm scheme, Chakravarthy and Osher's TVD; (i) second-order FCT of Zalesak; (j) eighth-order FCT of Zalesak; (k) MUSCL of Davis; (l) MUSCL of Colella; (m) ENO of Harten and Osher; (n) PPM of Colella and Woodward.

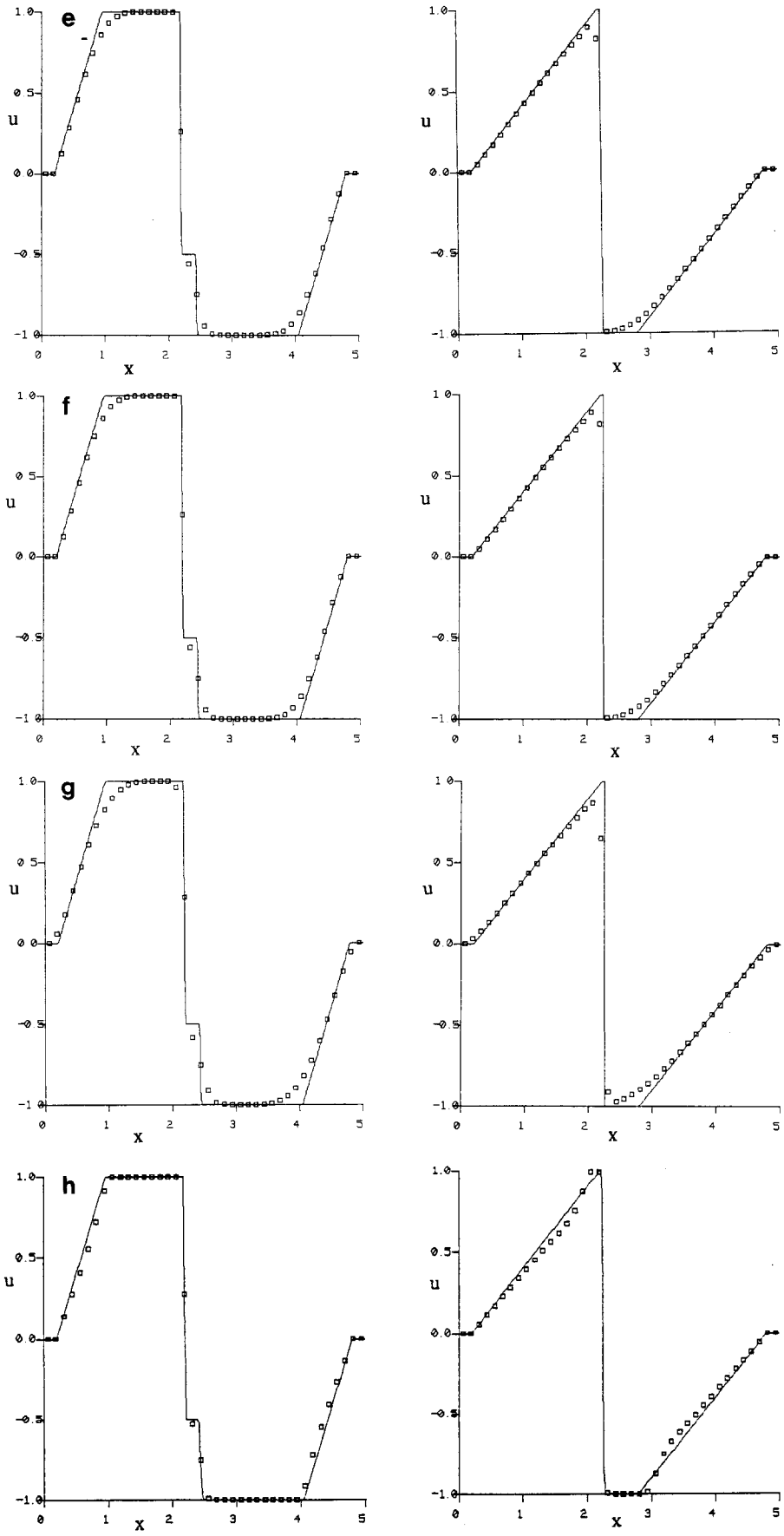

FIG. 5—*Continued*

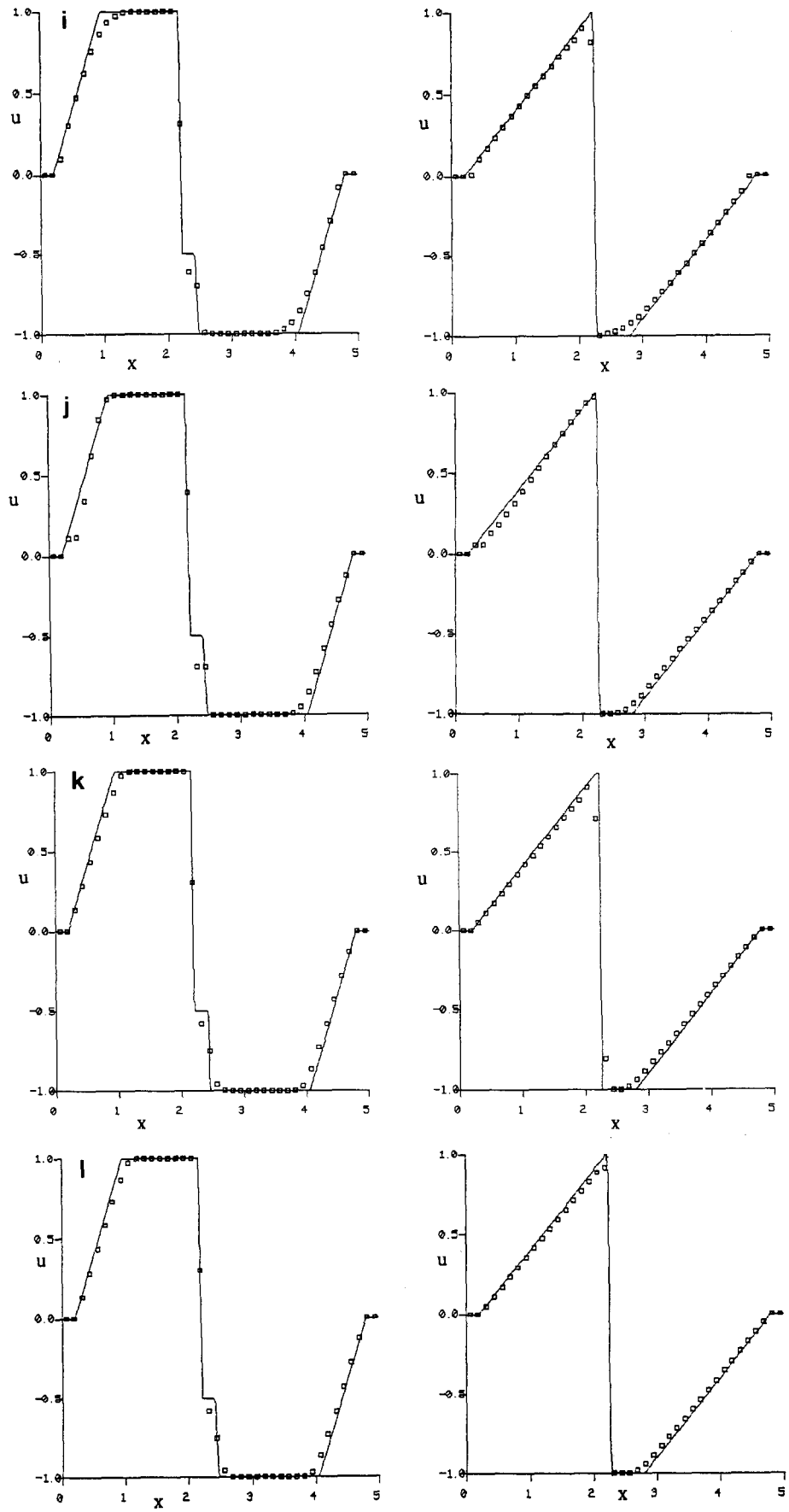

FIG. 5—*Continued*

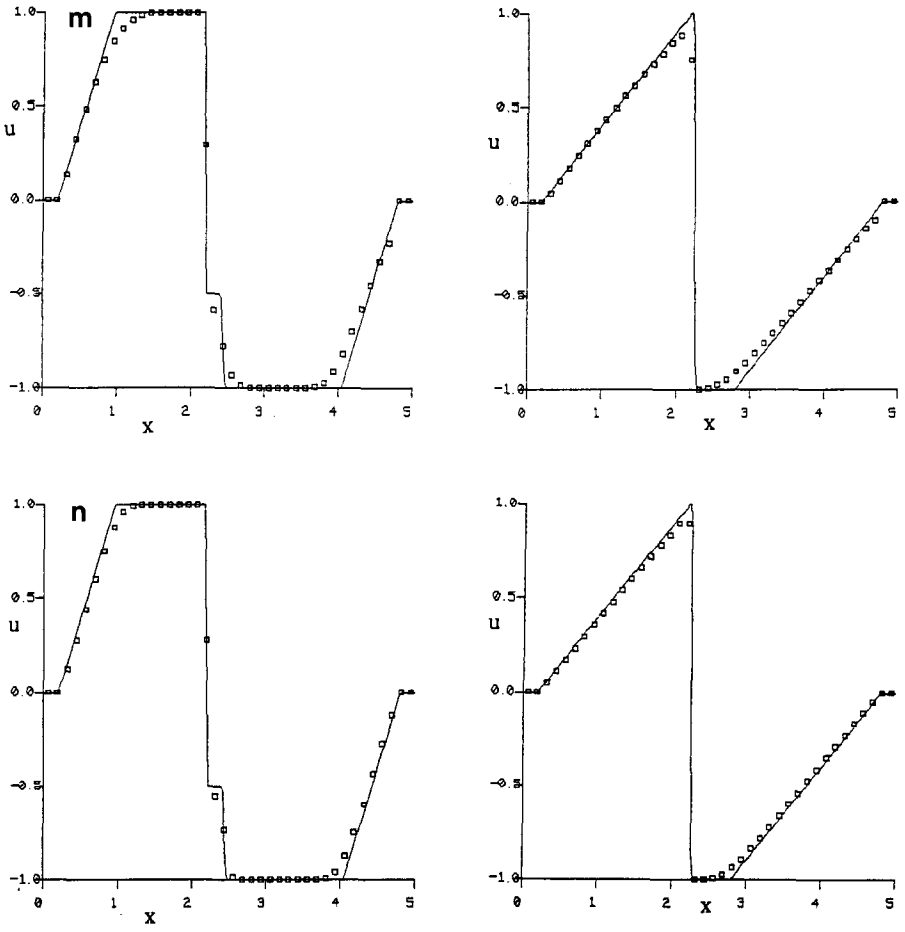

FIG. 5—*Continued*

comparable results with the TVD scheme. The high order scheme (Fig. 5j) would have been marvelous if it has no staircase. Davis' MUSCL gives two transition points across the shock (Fig. 5k). Colella's MUSCL (Fig. 5l) is excellent. ENO is diffusive (Fig. 5m), and PPM is still competitive (Fig. 5n).

4. SUMMARY AND CONCLUSIONS

The present study has systematically assessed all advanced numerical schemes for nonlinear scalar transport problems. Essential mathematical details of each scheme have been documented. Likewise, full details of test problems and results of various schemes have been described. Several advanced shock-capturing schemes have been applied to solve the nonlinear Burgers' equation to assess their ability in resolving sharp discontinuity, expansion zone, and propagation and collision of shocks.

A one-dimensional computer code has been written in which all of the known, advanced differencing schemes have been incorporated. The main conclusions from this study can be summarized as follows:

1. For discontinuous functions, the Warming–Beam scheme generates pre-shock wiggles, whereas the Lax–Wendroff scheme generates post-shock wiggles. When combined in the form of a TVD scheme with "intelligent" switching, a high resolution shock capturing scheme has been obtained. The switching was achieved by applying the limiters.

2. Some of the existing limiters, such as the superbee or MUSCL limiters, are more compressive than minimod or monotonic limiters. Compressive limiters capture discontinuities with fewer transition points. However, for moving and dissipating shocks and at locally smooth extrema, it may create artificial inflection points. For steady state problems the choice would be a compressive limiter, while for transient flows probably a more dissipative limiter would be preferred.

3. The performances of upwind TVD, symmetric TVD, and Roe and Sweby's TVD schemes are similar to each

other. Roe and Sweby's TVD, which has additional computational count in determining the direction of characteristic speed, usually performs better than symmetric TVD schemes, especially in the nonlinear problem.

4. Chakravarthy and Osher's TVD scheme requires

3. P. K. Sweby, *SIAM J. Num. Anal.* **21**, 995 (1984).
4. A. Harten, *J. Comput. Phys.* **49**, 357 (1983).
5. H. C. Yee, R. F. Warming, and A. Harten, *J. Comput. Phys.* **57**, 327 (1985).
6. H. C. Yee, *J. Comput. Phys.* **68**, 151 (1987).
7. H. C. Yee, "Upwind and Symmetric Shock-Capturing Schemes,"